Some other statistics which appear to be nearly independent of primary energy are:

(1) The average energy of the individual electrons lost because their energy is <10 MeV is 6.98 MeV.

(2) The average energy of photons with $E<10$ MeV is 0.909 MeV.

(3) The average energy of backscattered electrons with $E>10$ MeV is 14.0 MeV.

(4) The average energy of backscattered photons with $E>10$ MeV is 13.1 MeV.

(5) The average number of all photons produced per electron track length is 11.04.

These shower parameters are not only nearly independent of the energy but also of the nature of the primary particle. If one considers the development of showers from the point of equivalent remaining energy then once past the shower maximum the showers look essentially the same and are nearly independent of the nature of the primary particle and the magnitude of its primary energy. It should be remembered that the results presented are only averages of the showers considered. An individual cascade can exhibit wide variations.

A comparison between Wilson's results and those given in the present work is shown in Figs. 1 and 2, where we have plotted the number of electrons with energy >10 MeV due to primary electrons of energy 500 and 200 MeV (Fig. 1) against depth in the lead absorber measured in radiation lengths. Figure 2 shows the same results for primary photons. On the same figures we have plotted Wilson's results for the number of electrons with energy >8 MeV. The discrepancy is very large amounting to almost 100% at the maximum in the case of primary photon results. The discrepancy cannot be accounted for by the fact that in our case we are considering electrons with energy >10 MeV whereas Wilson considers particles with $E>8$ MeV. As we have already pointed out, the average energy of electrons with $E<10$ MeV is 6.98 MeV. Apparently Wilson's method of calculation gave too low an energy degradation for the electrons, thus accounting for the differences above.

PHYSICAL REVIEW VOLUME 128, NUMBER 5 DECEMBER 1, 1962

μ-Mesonic Atom Studies of Ti, Fe, Cu, Zn, Tl, Pb, and Bi†*

W. Frati‡ and J. Rainwater
Columbia University, New York, New York

(Received June 1, 1962)

This paper presents the results of a precision re-evaluation of the μ-mesonic x-ray transition energies for Tl, Pb, Bi, Ti, Fe, Cu, and Zn. The $2p-1s$ and $3d-2p$ transition regions were studied for Tl, Pb, and Bi, and the $2p$ fine structure splitting was determined with good precision from both sets of measurements. The Tl, Pb, and Bi transition energies were determined to about 0.2%, while the $2p$ state fine structure splitting was determined to within 2 to 3%. The results are in good agreement with the theoretically predicted values of Ford and Wills, based on the charge distributions implied from the high-energy electron scattering experiments. An anomaly in the observed intensity ratio of the $2p_{1/2}-1s$ to $2p_{3/2}-1s$ transitions for Bi and Tl is discussed. It is believed to be due to an excitation of the first excited state of the initial nucleus. The observed $2p-1s$ transition energies for Ti, Fe, Cu, and Zn are given, with experimental uncertainties of 0.2 to 0.3%. The comparison with the theoretically predicted values is much improved relative to the earlier experimental results.

I. INTRODUCTION

SINCE the original studies of the $2p-1s$ μ-mesonic x rays by Fitch and Rainwater,[1] we have at various times attempted to improve the precision of these results with respect to the $2p-1s$ transition energy for elements near $Z=82$. The earlier $2p-1s$ spectra for Tl, Pb, and Bi were of such a shape that a reasonable interpretation required an assumption of approximately the expected 190-keV fine structure splitting of the $2p_{3/2}$, $2p_{1/2}$ levels. However, the experimental curves had limited statistical accuracy, and the energy calibration using the 4.43-MeV γ ray from a Pu-Be source required a considerable energy and shape extrapolation, which limited the absolute accuracy of the energy evaluations.

In this paper we report new results for the $2p-1s$, and also for the $3d-2p$ x rays from Tl, Pb, and Bi, which we believe to be an order of magnitude superior to the earlier results. A much better absolute evaluation of the x-ray energies was obtained by use of a fast neutron irradiated circulating water target which yielded 6.134 ± 0.006-MeV γ rays, associated with a transition from a well-studied excited state of O^{16}. These x-ray energies are found to be in excellent agreement

† This research is supported by the Office of Naval Research.

* The adjective "mesonic" is retained here, even though the muon has lately been excluded from the meson family, since no satisfactory new label has been invented to cope with the situation. The term "μ-leptonic" or "muonic" are possible.

‡ Present address: University of Pennsylvania, Philadelphia, Pennsylvania.

[1] V. L. Fitch and J. Rainwater, Phys. Rev. **92**, 789 (1953).

with the latest theoretical values.[2] In addition, we were able to obtain precision evaluations of the $2p_{3/2}$, $2p_{1/2}$ fine structure splittings by independent least-square fitting of the $2p-1s$ spectra. The $2p-1s$ and $3d-2p$ transitions gave independent evaluations of the $2p$ splitting in excellent agreement with each other and with theory.

Over a period of two years we have had three major runs during which attempts were made to obtain a satisfactory resolution of the fine structure for Pb and its neighboring elements. The results of these separate attempts were all in substantial agreement and superior to the 1953 measurements.[1] There were, however, certain unsatisfactory aspects of the experimental curves obtained from the first two runs which, due to improvements in experimental conditions, were absent in the last series of runs. Only the last series is reported in this paper.

Measurements were also made of the $2p-1s$ x rays from Ti ($Z=22$), Fe ($Z=26$), Cu ($Z=29$), and Zn ($Z=30$). In general, less emphasis was placed on these measurements than those for Z around 82. The exception was the case of Fe, where the x-ray energy happened to be very near to that of the (1.2736 ± 0.0018) MeV γ ray from Na^{22}. With the exception of Fe, which was 1.3% higher than theoretical calculations, the other elements agreed to better than 1% with the theoretical calculations. Ti now falls within 1/2% of the calculated value, unlike the results of the 1953 measurements.[1] The principle factors of technological improvement since the 1953 studies are:

(a) A greatly improved shielding system between the Nevis synchrocyclotron and the detection area.

(b) Development of a vibrating target "beam stretcher" which gave a greatly improved duty factor.

(c) The use of γ-ray detector which consisted of a 3-in. diam by 3 in. long NaI crystal surrounded by a 5-in.-long NaI annulus shell of 2-in. radial thickness used in anticoincidence with the center crystal.

(d) Improved beam optics enabling us to stop 500 muons per sec.

(e) The use of two Penco 100-channel analyzers operating simultaneously, with one being used for the mesonic x rays, and the other for a lower energy γ-ray monitor which enabled us to check and correct for any drifts in detector sensitivity.

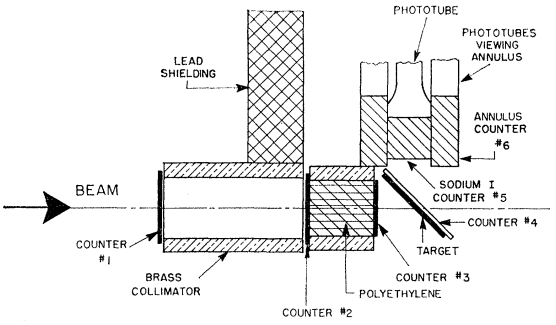

FIG. 2. Counter telescope.

II. EXPERIMENTAL ARRANGEMENT

A. Muon Beam

The floor plan of the cyclotron, main shielding wall, and experimental area is shown in Fig. 1. The mesons are produced internally when the 385-MeV proton beam strikes a vibrating target[3] which is used as a beam stretcher. By also turning off the cyclotron rf after the protons reach the proper radius the meson production is stretched over approximately 25% of the operation cycle as contrasted to 2% previously. A magnetic channel between the cyclotron chamber and the shielding wall permits the extraction of 45-MeV pions and muons of nearly the same momentum (60 MeV) through a beam aperture in the shielding wall. The shielding wall in this region now consists of 10 ft of steel over most of its height with a 15-in.-thick facing of borax loaded concrete in steel boxes. Shielding structures on the experimental floor are now based on the use of a large number of surplus U. S. Navy steel barbettes, formerly battleship gun turret armor, which are 6 in. thick and about 13 ft high by 13 ft horizontal length curved in an arc of 1/5 of a circle so that they are stable when standing erect. The arrangement of these barbettes is shown in Fig. 1, which does not show the additional roof shielding of heavy steel plates over the "experimental house." After emerging from the main shielding wall the beam was bent and further defined by a dipole magnet followed by two quadrupole magnets, after which it entered the experimental house through holes in the shielding array at its front. The character of the beam was affected by varying the meson target

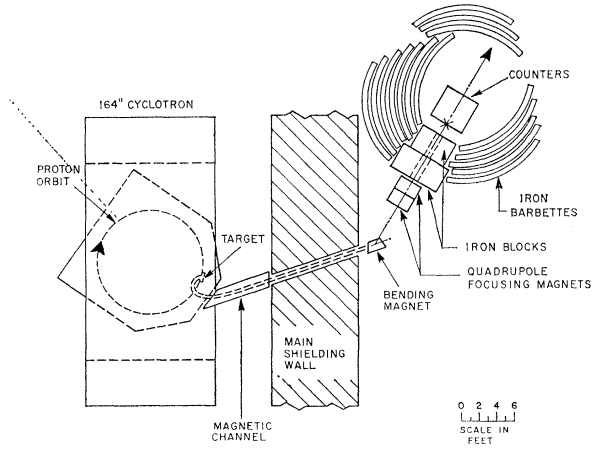

FIG. 1. Floor plan.

[2] K. W. Ford and J. G. Wills, Los Alamos Scientific Laboratory Report LAMS-2387, March 1960 (unpublished).

[3] J. Rosen, Columbia University, Nevis Report No. 92 (unpublished).

position and the dipole and quadrupole currents. We chose to compromise between muon intensity and muon purity and operated with a beam incident to our counter telescope which was approximately 20% muons, 30% pions, and 50% electrons. This was determined by using a modification of the counter arrangement shown in Fig. 2, which permitted a coincidence measurement of stoppings in a $\frac{1}{2}$-in. polyethylene target ($123\bar{4}$), and a coincidence measurement of delayed electrons resulting from the decay of the stopped μ^- mesons. The upper curve in Fig. 3 shows the differential range curve ($123\bar{4}$), with excellent separation of pions and muons. The lower curve shows the delayed μ^- decay electron coincidence rate. With a $\frac{1}{8}$-in. Pb target, and the geometry depicted in Fig. 2, a muon stopping rate ($123\bar{4}$) of 500 per sec was achieved.

B. Detection System

The detector system arrangement is shown in Fig. 2, in the manner used during the detection of the mesonic x rays. The system rests on a table which contains an elaborate system for blowing filtered temperature controlled air ($\pm 1/2$°F) on the NaI crystals. Considerable extra shielding structures were stacked around the muon path and NaI crystals to prevent unwanted scattered particles from reaching the NaI detectors. This was important in obtaining a final large reduction of high-energy (>10 MeV) general background in the center crystals. With the beam on, this rate was reduced to approximately 20 per sec. With the monitor source in the system the average counting rate of the center crystal with the beam on was 1000 per sec of which 300 per sec was due to the beam, for energies greater than $\frac{1}{2}$ MeV. The remainder was mainly due to the monitor γ-ray source.

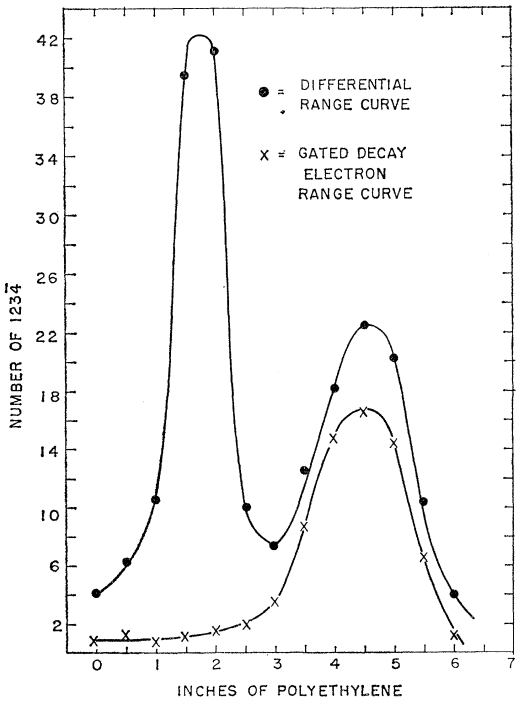

FIG. 3. Range curves.

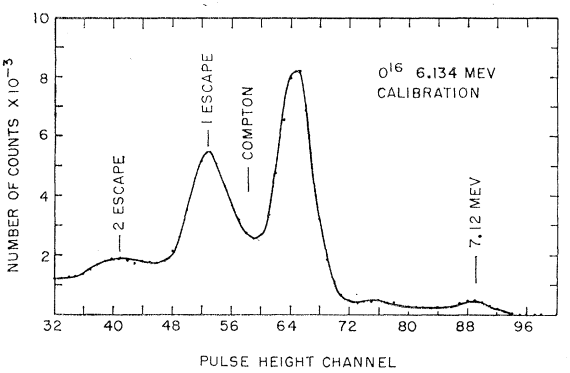

FIG. 4. Response of the 3-in.×3-in. NaI crystal with the annular counter used in anticoincidence, to the 6.134-MeV γ ray from O^{16}.

With the exception of the NaI counters, all of the counters indicated in Fig. 2 used plastifluor scintillators viewed by 6810A phototubes. The dimensions of all counters are given in Table I.

During the mesonic atom runs the annulus NaI counter was used in anticoincidence to reduce background and to discriminate against the one- and two-escape peaks and Compton scattering in the center crystal, where the full energy of the incident γ ray is not released in the center crystal.

This greatly simplifies the response of the γ-ray detection system for 6-MeV photons, since only 10% of the incident γ rays will lose their full energy in the center crystal at 6 MeV, and 25% at 2.5 MeV. This simplification of the pulse-height-spectrum shape for monochromatic photons greatly improves one's ability to interpret the observed response when photons of more than one energy contribute as is the case, due to the fine structure, for the $2p-1s$ and $3d-2p$ transitions. The $3d-2p$ transition spectra are also improved because of the reduction of the usual Compton scattering "tail" from the higher energy $2p-1s$ x rays.

C. Na^{24} and O^{16} Sources

Figure 4 shows the calibration response to the fast-neutron-irradiated circulating water source of 6.134-

TABLE I. Dimensions of counters.

Counter	Type	Dimensions
1	Plastifluor	5 in.×5 in.×$\frac{3}{8}$ in.
2	Plastifluor	5 in.×5 in.×$\frac{3}{8}$ in.
3	Plastifluor	4 in.×4 in.×$\frac{3}{8}$ in.
$\bar{4}$	Plastifluor	7 in.×7 in.×$\frac{3}{8}$ in.
5	NaI(Tl)	3 in. diam×3 in. thick
$\bar{6}$	NaI(Tl)	3 in. i.d.×7 in. o.d.×5 in. long

MeV γ rays[4] (hereafter called the "O^{16} source") of the γ-ray detector. The two-escape peak is quite small and the one-escape peak is greatly reduced relative to the full-energy peak by the annulus (approximately a factor of 4). This O^{16} source was obtained as follows. A 1 ft by 1 ft by 4 in. water tank was mounted just outside the cyclotron chamber with the 1 ft by 1 ft area facing the forward cone of neutrons generated in the meson target. An $O^{16}(n,p)N^{16}$ reaction takes place. The N^{16} undergoes β decay with a 7.3-sec half-life to O^{16} with 26% directly to the ground state, 68% to the 6.134-MeV 3^- excited state, 5% to the 7.12-MeV level, and 1% to the 8.88-MeV excited state. The 8.88-MeV state decays via the 7.12-, 6.9-, and 6.134-MeV states in the ratio of 3:1:30. The 7.12- and 6.134-MeV levels decay directly to the ground state. Thus, one observes 6.134- and 7.12-MeV γ rays in a ratio of 13:1. The weak presence of the 7.12-MeV γ ray was later subtracted analytically to obtain a "pure" 6.134-MeV γ-ray response curve.

The neutron activated water containing the N^{16} was pumped at a high speed via $\frac{1}{2}$-in. plastic hose to the final "source box", the transit time being about 4 sec, which provides an adequate γ-ray intensity at the source box.

The source box was 4 in. by $5\frac{3}{4}$ in. by 1 in. thick with $\frac{1}{32}$-in. brass side walls. This area was selected to simulate the targets and the thickness was chosen to simulate the Compton scattering of the target. The return path from the source box to the water tank was $\frac{1}{2}$-in. plastic hose for the first ten feet and then 1-in. hose was used for the remainder of the return path. The $\frac{1}{2}$-in. plastic hoses were attached at 45° to the plane of the source box so that they leave at 90° with respect to the faces of the NaI crystals. This was done to maximize the box to hose contributions to the counting rate. This source box was always mounted at the target position when calibrations were taken to simulate, as nearly as possible, the environment conditions of target sources of μ-mesonic x rays.

Figure 5 shows the response to a Na^{24} calibration source.[5] This was produced by exposing a saturated NaCl solution to the cyclotron. The measurements were always made using the solution in a 4 in. by $5\frac{3}{4}$ in. by 1 in. plastic container placed at the target position.

D. Electronics

The block diagram for the electronics is shown in Fig. 6. The pulses from counters 1, 2, and 3 were clipped to 10 nsec. The pulse from the anticounter $\bar{4}$ was stretched to 30 nsec. These four pulses were fed into a Garwin-type coincidence circuit from which (12), (123), and (123$\bar{4}$) coincidences were derived. The (123$\bar{4}$) pulse was 50 nsec wide and was used to define a muon stopping. This pulse is referred to as μ_s.

Two pulses are derived from the 3-in. phototube that views the 3 in. by 3 in. center NaI crystal. One for pulse-height analysis was taken from the next to last dynode. This was shaped to have a 0.2-μsec rise and a 7-μsec decay, to meet the requirements of a Hamner non-overload linear amplifier. This is referred to as the slow 5 pulse. The second pulse, derived from the collector, is clipped to 100 nsec. This pulse is referred to as 5. The pulse derived from the annulus NaI counter is the sum of the signals from the six 2-in. phototubes which view the crystal. This pulse is also clipped to 100 nsec and is referred to as 6.

The three pulses μ_s, 5, and 6 are amplified and then fed into tunnel diode discriminators which are triggered on the rise of these pulses. The tunnel diode pulses are used to generate 10-nsec pulses for μ_s and 5 and a 200-nsec pulse for 6. These three pulses are the inputs for a simple diode coincidence circuit which yields (μ_s-5-$\bar{6}$) and (5-$\bar{6}$) pulses. The (μ_s-5-$\bar{6}$) are interpreted as events where a μ^- stopping is accompanied by a properly detected photon.

Cable lengths are adjusted to give proper relative positioning of the pulses in time at the coincidence circuits. Varying the relative μ_s to 5 delay yielded a 25-nsec flat region with a 2-nsec falloff width on either side for photon energies of 1 to 10 MeV. To reduce the effect of μ^- capture γ rays from Tl, Pb, and Bi the 5 pulse was set at 7 nsec from its greatest delay within the flat response region. Taking[6] 70 nsec for the observed mean life for the muon capture for Z around 82 we discriminate against 90% of the events where a capture γ ray, but not a prompt x ray, is detected.

A running time of approximately 24 h each was spent

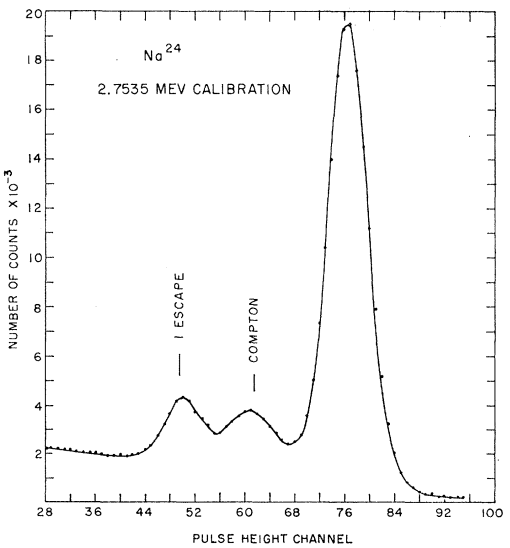

FIG. 5. Response of the 3-in.×3-in. NaI crystal with the annular counter used in anticoincidence, to the 2.7535-MeV γ ray from Na^{24}.

[4] F. Ajzenberg-Selove and T. Lauritsen, Technical Report (to be published).

[5] A. Hedgran and D. Lind, Arkiv Fysik **5**, 177 (1952).

[6] J. C. Sens, Phys. Rev. **113**, 679 (1959).

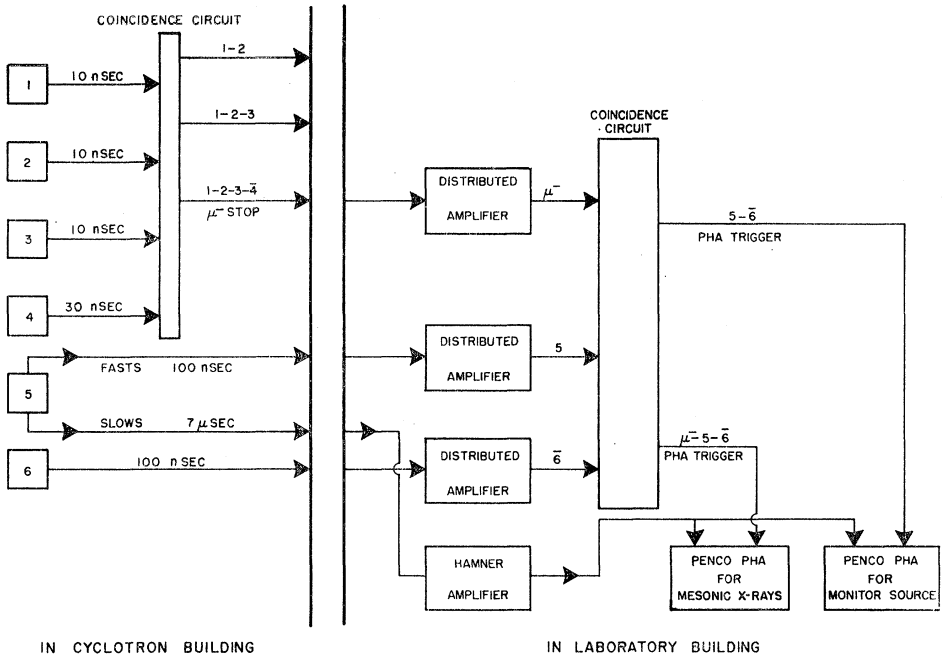

FIG. 6. Block diagram of electronics.

on the $2p-1s$ transitions for Pb, Bi, and Tl. Since the fine structure splitting is only 3% it is necessary for the photon detection system to have very good pulse height stability over this time interval. This includes the phototube, the high voltage to the phototube, preamplifier, Hamner amplifier, and the Penco pulse-height analyzer (P.H.A.). It was found extremely difficult to maintain better then 1% long range stability over 24 h. To circumvent this difficulty, the following procedure was used. Drifts were kept to a minimum by blowing temperature controlled air ($\pm 1/2°$F) on the NaI crystals and preamplifier. A γ-ray source was then placed near the crystal to serve as a monitor on the drifts. The (5-$\bar{6}$) coincidence pulses triggered one 100-channel Penco P.H.A. The (μ_s-5-$\bar{6}$) pulses triggered another 100-channel P.H.A. Both units analyzed pulses coming from the same Hamner amplifier. Thus, any drift, anywhere along the line from the NaI crystal up to but not including the two P.H.A.'s was identical for the reference γ ray in the first P.H.A., and mesonic x rays and calibration γ rays in the second P.H.A. The relative drifts of the two P.H.A. were monitored with frequent calibrations using a standard mercury relay pulse generator. Relative drifts were thus detected. The separate short runs were combined using a procedure which eliminated drift effects to 0.1% or better. Since the reference lower energy γ-ray spectrum was also taken during the times when the higher energy calibration (O^{16} or Na^{24}) γ-ray spectrum was measured, this 0.1% figure also applies to the intercomparison of the calibration γ-ray measurement and the mesonic x-ray measurements. The calibration γ-ray measurements were made at adjacent time periods to the mesonic x-ray measurements.

E. Procedure

1. 2p—1s Tl, Pb, and Bi

Co^{60} was used for the γ-ray monitor source. It gives γ rays of 1.17 and 1.33 MeV, both of which are well below the 6-MeV γ ray arising from the $2p-1s$ transitions in Tl, Pb, and Bi. The Tl target was 3 in. by $5\frac{3}{4}$ in. by $\frac{1}{8}$ in. The Pb and Bi targets were 4 in. by $5\frac{3}{4}$ in. by $\frac{1}{8}$ in.

Approximately 50 runs of 30 min each were taken for each element. The statistical accuracy of the Co^{60} spectrum obtained during each 30 min count was sufficient to define a relative energy scale to $\pm 0.04\%$. Approximately 1000 total peak x-ray counts in an energy interval 0.04 MeV wide were accumulated. This is sufficient to position the spectrum to approximately $\pm 0.1\%$ relative to the known energy calibration. The first and last run of each series was a (6.134 ± 0.006)-MeV calibration.

To be certain that μ^- capture γ rays wouldn't affect the $2p-1s$ spectrum a run was made to examine the shape and intensity of the capture γ-ray spectrum. The μ_s pulse was delayed 70 nsec and a 200-nsec gate was opened. Any 5-$\bar{6}$ coincidence arriving in this time interval triggered the mesonic atom P.H.A. The 70-nsec delay corresponds to a 45-nsec delay from the time a muon stops since the cable curve is 25 nsec wide. Thus, approximately 50% of the capture γ rays were counted. The delayed (μ_s-5-$\bar{6}$) coincidence rate was down a factor of 100 for Bi, and 50 for Tl and Pb, from the mesonic atom x-ray rate, with no well-defined capture γ rays being present in the region of 3.5 to 8.0 MeV.

2. 3d—2p Pb, Bi, Tl

The procedure here is the same as for the $2p-1s$ run with the following three exceptions:

(a) The 2.7535±0.001 MeV γ ray[5] from radioactive Na^{24} was used for the energy calibration.

(b) The 661-keV γ ray of Cs^{137} was used for the monitor source.

(c) Approximately 20 runs of 1 h each were taken.

This allowed about 1000 counts to be accumulated in the peak of the spectrum using 0.02-MeV energy intervals. This again was sufficient to determine the position of the $3d-2p$ mesonic atom spectrum to approximately ±0.1% relative to the calibration spectrum.

The capture γ rays in the $3d-2p$ energy region (1.5 to 3.0 MeV) were investigated in the same manner as was done for the $2p-1s$ energy region. The delayed coincidence rate was down a factor of 2.5 for Pb and Tl and 2.0 for Bi from the x-ray counting rate. No well-defined capture γ rays were observed for Pb and Tl. However, a very pronounced capture γ ray of approximately 2.6 MeV was observed for Bi^{209}. This spectrum is shown in Fig. 7, and is discussed in more detail in a later section.

3. 2p—1s Fe

The iron target was 4 in. by $5\frac{3}{4}$ in. by $\frac{1}{8}$ in. Due to the increased efficiency of detecting the full energy of a 1-MeV γ ray, only five runs of 1 h each were necessary to reach 1000 peak counts using 10-keV energy intervals. The monitor source was Cs^{137}, and the calibration source was Na^{22} which has a (1.2736±0.0018)-MeV γ ray.[7] Capture γ rays were searched for with no well-defined energies being observed. The μ^- capture rate was down by a factor of 2.5 from the mesonic atom x-ray rate in the energy interval covered.

4. 2p—1s Zn

The method for zinc was the same as for Fe. Again, no well-defined γ-ray peaks were observed.

5. 2p—1s Cu

The procedure was the same as for the $2p-1s$ Fe and Zn runs, with the addition that the (1.3679±0.001)-MeV γ ray from Na^{24} was used along with the 1.2736-MeV Na^{22} γ ray. This served as a check on the technique of normalizing individual runs to the relative positions of the monitor source, and on the energy linearity of the system. The $2p-1s$ energy was calculated separately for each calibration source, and excellent agreement was obtained.

6. 2p—1s Ti

The titanium target was 6 in. by 6 in. by $\frac{1}{4}$ in. The monitor source was Cs^{137}. The calibrating sources were Cs^{137} and the 0.845-MeV γ rays[8] from Mn^{56}. The Mn^{56} was obtained by exposing a saturated solution of $MnCl_2$ to neutrons near the cyclotron chamber. The $2p-1s$ energy was calculated separately using the two calibration sources with excellent agreement for the two calibrations. No capture γ rays were observed.

[7] P. P. Singh, H. W. Dosso, and G. M. Griffiths, Can J. Phys. **37**, 1055 (1959).

[8] M. Sakai, J. L. Dick, W. S. Anderson, and J. D. Kurbatov, Phys. Rev. **95**, 101 (1955).

III. ANALYSIS OF THE DATA

A. $2p-1s$ for Tl, Pb, and Bi

At the time when the analysis of the many 30-min runs was to be carried out, the following information was available: the mesonic atom x-ray spectrum counts per channel and the monitor γ-ray spectrum counts per channel for each 30-min run. Similar information for the O^{16} calibration γ ray and the monitor γ ray was known for a run at the beginning and end of each series. At the beginning of each series a standard pulse generator, linear to 0.1%, was used at the input of the Hamner amplifier to determine the relative pulse height corresponding to the beginning of each channel for each P.H.A. A similar check for relative drifts of the two P.H.A.'s was made at the end of each series and about every 4 h during the series. This last information determined the ratio of γ-ray energies corresponding to the beginning of different channels in the same and the opposite P.H.A.'s.

The individual runs in a series were then folded by the following method. One of the runs was chosen as a standard for the series. The pulser calibration determines the relative pulse heights of the beginning and end of the nth channel for both P.H.A.'s. As drifts occurred, a given pulse height corresponded to a different energy. These drifts were detected and measured to within ±0.1%, relative to the standard run, using the relative positions of the γ-ray monitor spectrum together with the relative calibration of the two P.H.A.'s. One thus knows the fractional drift (d_j) of the jth run relative to the standard run. This number was now applied to the x-ray data. The nth channel of the x-ray P.H.A. for the standard run covered a pulse-height interval $P_{n,0}$ to $P_{n+1,0}$, corresponding to a given energy interval. The same pulse-height interval covered a different energy interval for the jth run. The fractional energy

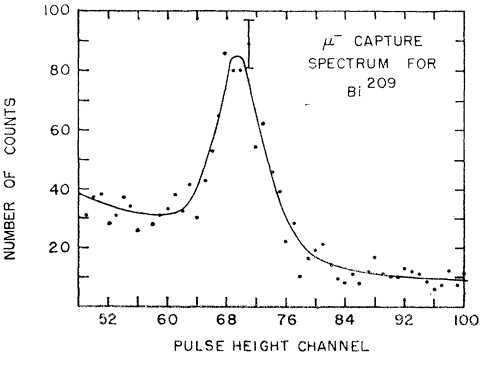

FIG. 7. γ-ray spectrum from μ^- capture in Bi^{209}.

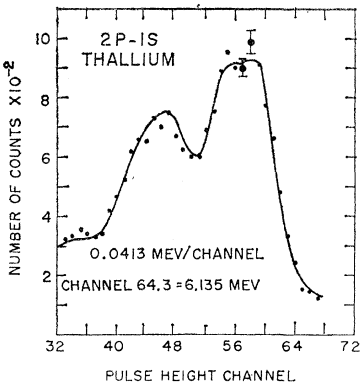

FIG. 8. Experimental results for the $2p-1s$ transition in Tl. The smooth curve represents the best-fit synthesized curve for which $\chi^2=28.7$.

overlap ($f_{m,n,j}$) of the mth interval of the jth run with the nth interval of the standard run was readily determined from d_j. Then $f_{m,n,j}$ times the number of counts in the mth interval of the jth run were placed in the standard nth interval for folding purposes. The runs using the O^{16} calibration γ ray were similarly treated.

The contribution of the 7.12-MeV γ ray from the O^{16} source spectrum was removed by assuming that its shape was similar to that for the 6.134-MeV γ ray except for the shift to higher energy. Thus 1/13 of the calibration spectrum was taken, raised 0.985 MeV in energy and subtracted from the original spectrum to obtaining a resulting "pure" 6.134-MeV calibration spectrum. This exact same spectrum shape was assumed to apply also for a single γ ray of the energy of the $2p_{3/2}-1s$ and the $2p_{1/2}-1s$ transitions. This was accomplished by displacing the reference spectrum a given number of channels equal to the energy difference (E_r-E) of the reference γ-ray (6.134 MeV) and assumed x-ray energies.

An attempt was then made to synthesize a match to the observed x-ray spectrum by assuming that the x-ray spectrum contained two photons of energy $E_{3/2}$ and $E_{1/2}$ each having the shape of the corrected O^{16} spectrum with relative weightings of $W_{3/2}$ and $W_{3/2}W$, plus a background. W is the relative weighting of the two photons and $W_{3/2}$ is the factor by which the shifted synthesized spectrum must be multiplied to generate the $E_{3/2}$ line contribution to the x-ray spectrum. The background was assumed to be a linear function of energy $(a+bE_n)$ over the energy region being analyzed. Then a, b, $(E_r-E_{3/2})$, $(E_{3/2}-E_{1/2}=\Delta_{2p})$, $W_{3/2}$, and W were made six free parameters in the following analysis.

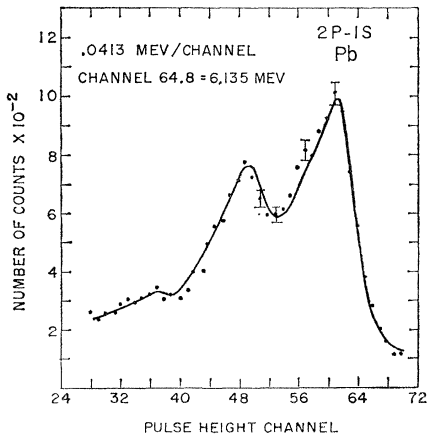

FIG. 9. Experimental results for the $2p-1s$ transition in Pb. The smooth curve represents the best-fit synthesized curve for which $\chi^2=27.7$.

A least-squares test of fit was made using a region of about 35 adjacent channels of the x-ray spectrum, essentially as indicated by the region covered in Figs. 8–10. The six free parameters were denoted as X_j. Denoting the x-ray spectrum and synthesized spectrum for the ith interval by N_i and F_i, respectively, then the least-squares analysis was made using the χ^2 function defined by

$$\chi^2=\sum_{i=1}^{35}\frac{(N_i-F_i)^2}{\sigma_i^2},$$

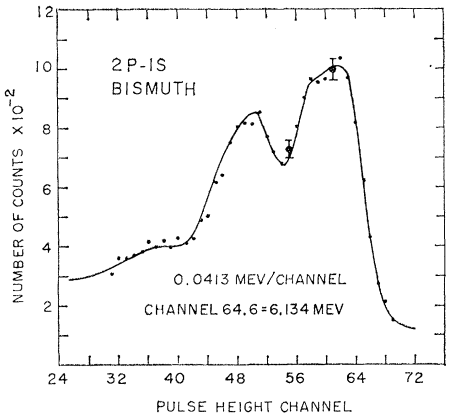

FIG. 10. Experimental results for the $2p-1s$ transition in Bi. The smooth curve represents the best-fit synthesized curve for which $\chi^2=26.7$.

where $\sigma_i^2=N_i+G_i$ is the uncertainty in (N_i-F_i) due to the statistical uncertainties in N_i and F_i. The term G_i which is much smaller then N_i represents the net contribution to σ_i^2 due to the limited statistical accuracy of the synthesized spectrum. χ^2 is assumed to have a quadratic dependence on the six X_j in the region of the best fit.

$$\chi^2=\sum_{j,k=1}^{6}\alpha_{jk}X_jX_k+\sum_{j=1}^{6}\beta_jX_j+\beta_0,$$

where $\alpha_{jk}=\alpha_{kj}$, β_j and β_0 are to be determined. This involves 28 independent coefficients, necessitating the computation of χ^2 for 28 combinations of the X_j, in the region of a rough best fit. The best fit is determined from the minimum of the assumed quadratic χ^2 function. The statistical uncertainty $(\Delta X_j)^2$ for this best fit is determined from the diagonal elements $(\alpha^{-1})_{rr}$ of the inverse matrix of α_{jk}. The data processing was done with the aid of an IBM-650 computer.

TABLE II. Theoretical and experimental results for $2p-1s$ and $3d-2p$ transitions in Tl, Pb, and Bi. Energies in MeV.

	$2p-1s$					$3d-2p$				
	$E(2p_{3/2}-1s)$		Δ_{2p}		W	$E(3d_{5/2}-2p_{3/2})-0.1\Delta_{3d}$		$\Delta_{2p}-0.9\Delta_{3d}$		W
Elements	Exp	Theor	Exp	Theor	Exp	Exp	Theor	Exp	Theor	Exp
Tl, $Z=81$	5.930±0.011	6.001±0.050	0.1876±0.0043	0.1843	0.97±0.09	2.458±0.005	2.452	0.146±0.005	0.1475	0.53±0.03
Pb, $Z=82$	5.990±0.011	6.025±0.050	0.1859±0.0060	0.188	0.49±0.07	2.498±0.004	2.502	0.147±0.004	0.1494	0.51±0.02
Bi, $Z=83$	6.053±0.009	5.995±0.050	0.1895±0.0042	0.188	0.75±0.05	2.555±0.004	2.538	0.148±0.004	0.1478	0.59±0.02
Bi,[a] $Z=83$		6.047±0.050		0.191			2.550		0.151	

[a] Suggested modified theoretical values as discussed in the text.

To the above statistical uncertainties one must add the contribution due to (a) the energy uncertainty of the calibration source, (b) the errors in the pulser calibrations, (c) the errors in determining the peak channel of the calibration γ-ray spectra, and (d) the errors in the relative energy scale between the folded x-ray runs and folded calibration runs established via the intermediary of the monitor γ-ray spectra. The x-ray energy E_m in terms of the calibration source reference energy E_r is $E_m=E_r(1-\rho/P_r)$, $\rho=(P_r-P_m)\ll P_r$ where P_r is the pulser calibration of the peak channel for the calibration spectrum, and P_m is a similar quantity for the $2p_{3/2}-1s$ x ray. The magnitude of P_r was obtained by trying to determine the position of the peak of the calibration γ-ray spectrum. Fortunately, an uncertainty as large as 1% in P_r contributes only 0.024% uncertainty in E_m for Pb, since $\rho/P_r=0.024$. The value of ρ was determined from the χ^2 analysis, along with its statistical uncertainty. ρ also has an uncertainty arising from the measurement of the slope of the pulser calibration vs channel number. This is negligible for the $2p-1s$ transitions due to the fact that ρ/P_r is so small. This does, however, make a contribution to the $3d-2p$ error calculations since ρ/P_r is, for example, 0.092 for Pb. The χ^2 analysis of the $2p-1s$ Pb transitions determines ρ to ±0.15 channels which yields a $\pm(0.108\%)$ uncertainty in E_m. If an additional conservative value of $\pm0.1\%$ is taken for the maximum uncertainty in the relative positioning of the reference and x-ray spectra via the intermediary of the monitor γ ray, a net uncertainty of $\pm0.15\%$ (0.0090 MeV) results from effects other than the uncertainty in $E_r=6.134$ MeV which is quoted to ±0.006 MeV at present. The small absolute uncertainty in E_r contributes significantly to the net uncertainty in E_m, but gives no significant contribution to the uncertainty in Δ_{2p}, to which only the statistical errors calculated from the χ^2 analysis make a significant contribution. The results and errors are listed in Table II. A breakdown of the contributions to the errors is given in Table IV.

The χ^2 analysis used 38 channels for Pb, 35 for Tl, and 38 for Bi.

The minimum χ^2 value for Pb was 27.7 compared with an expected 32 ± 8. The minimum χ^2 for Tl was 28.7, compared with an expected 29 ± 7.6. The minimum χ^2 for Tl was 28.7, compared with an expected 29 ± 7.6. The minimum χ^2 for Bi was 26.7 compared with an expected value of 32 ± 8. The minimum χ^2 values are thus satisfactorily close to the expected values. The only unexpected result is that the best-fit value of the ratio W of the $E_{1/2}$ to $E_{3/2}$ intensities was further from the predicted value of 0.50 than expected. In particular, the best fit W values are significantly different for Tl, Pb, and Bi being 0.97 ± 0.09, 0.49 ± 0.07, 0.75 ± 0.05, respectively. Independent information on the relative number of transitions to the $2p_{3/2}$ and $2p_{1/2}$ levels was obtained from the $3d-2p$ spectra, which is in agreement with the expected value of 0.50. The matter is discussed in more detail in a later section.

B. $3d-2p$ for Tl, Pb, and Bi

This analysis is similar to that for the $2p-1s$, with the exception that the calibration used the 2.7535-MeV spectrum from Na^{24}. The $3d-2p$ transitions have three energies corresponding to $3d_{5/2}\rightarrow 2p_{3/2}$, $3d_{3/2}\rightarrow 2p_{1/2}$, and $3d_{3/2}\rightarrow 2p_{3/2}$. Ignoring the relatively small energy difference of these transitions, one expects relative state statistical weightings to go as $(2J+1)$. This predicts relative intensities of 9, 5, 1, respectively, for the three transitions. Since the expected $3d$ state splitting is small (0.04 MeV), and is not expected to be influenced significantly by the finite nuclear size, the $3d_{5/2}\rightarrow 2p_{3/2}$ and the $3d_{3/2}\rightarrow 2p_{3/2}$ are treated as one γ ray with an intensity $1/W$ times that of the $3d_{3/2}\rightarrow 2p_{1/2}$ transitions. Thus, the energy that is determined from the χ^2 analysis is the $3d_{5/2}\rightarrow 2p_{3/2}$ energy less 0.1 times the $3d$ state splitting. Similarly, the energy difference obtained from the χ^2 analysis is the $2p$-state splitting less 0.9

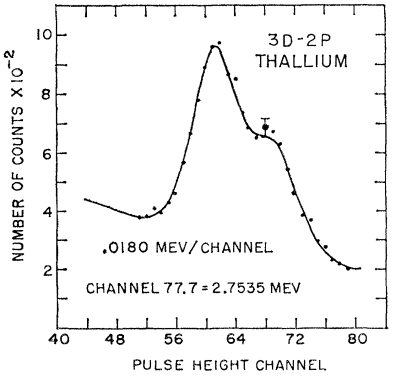

FIG. 11. Experimental results for the $3d-2p$ transitions in Tl. The smooth curve represents the best-fit synthesized curve for which $\chi^2=11.7$.

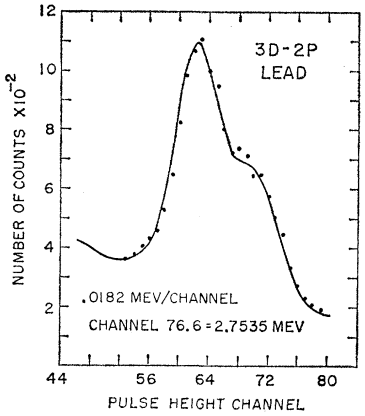

FIG. 12. Experimental results for the $3d-2p$ transitions in Pb. The smooth curve represents the best-fit synthesized curve for which $\chi^2=12.7$.

times the $3d$-state splitting. These are denoted by $(E_{5/2\to3/2}-0.1\Delta_{3d})$ and $(\Delta_{2p}-0.9\Delta_{3d})$.

The experimental results for the $3d-2p$ transitions of the Tl, Pb, and Bi are shown in Figs. 11, 12, and 13, respectively, along with the best fit synthesized curves. The χ^2 analysis for Tl was taken over a 25-channel interval with the minimum χ^2 being 11.7 compared to the expected value of 19 ± 6.2. The χ^2 analysis for Pb was taken over a 25-channel interval with the minimum χ^2 being 12.7. The χ^2 analysis for Bi covered a 28-channel interval with the minimum χ^2 being 13.1 compared to the expected value of 22 ± 6.6.

In addition to the uncertainties discussed previously, there is an additional systematic correction and uncertainty due to the difference in resolution of the 2.7535-MeV calibration γ ray and the mesonic atom x rays. This is because the x-ray energy is significantly lower than the calibration energy ($\rho/p_r=0.092$ for Pb) for the $3d-2p$ transitions, whereas $\rho/p_r=0.024$ for the $2p-1s$ transitions in Pb. The resolution of the 2.7535-MeV γ ray is measured to be 5.3% which is 0.146 MeV wide between the half-points. Using the square root of the ratio of the energies, one expects a 5.6% resolution for a 2.50-MeV γ ray, which is 0.139 MeV wide. If the percentage resolution were independent of energy a 2.50-MeV γ ray would be only 0.133 MeV wide. Thus, the calibration curve that was slid down to represent the 2.50-MeV $3d_{5/2}-2p_{2/3}$ transition x rays is approximately 0.007 MeV too wide assuming a $\sqrt{E}$ resolution function, or 0.013 MeV too wide assuming the resolution is energy independent. We shall work with the $\sqrt{E}$ dependence, which is closer to reality. Similarly the $3d_{3/2}\to2p_{1/2}$ transition will be represented by a calibration spectrum that is 0.003 MeV too wide. Thus, to the $(\Delta_{2p}-0.9\Delta_{3d})$ value obtained from the χ^2 analysis the value of $\frac{1}{2}$ (0.007+0.003) MeV is added. Similarly, the value of 0.0035 is subtracted from the χ^2 determined value of $(E_{5/2\to3/2}-0.1\Delta)$.

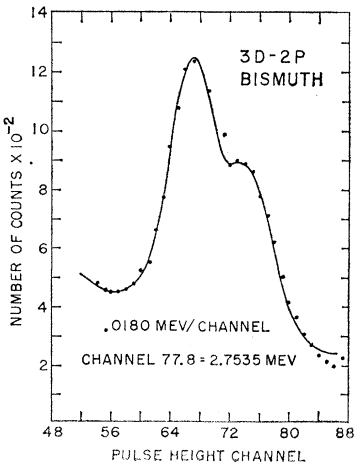

FIG. 13. Experimental results for the $3d-2p$ transition in Bi. The smooth curve represents the best-fit synthesized curve for which $\chi^2=13.1$.

TABLE III. Theoretical and experimental results for $2p-1s$ transitions in Ti, Fe, Cu, and Zn. Energies in MeV.

Element	Z	$2p-1s$ (Exp)	$2p-1s$ (Theor)	Calibrating source and energy	
Ti	22	0.9247±0.0025	0.9198±0.003	Cs^{137}	0.6616[a]
Ti	22	0.925 ±0.015		Mn^{56}	0.845[b]
Fe	26	1.2555±0.0024	1.2393±0.006	Na^{22}	1.2736[c]
Cu	29	1.5082±0.0040	1.4965±0.007	Na^{24}	1.3679[d]
Cu	29	1.5064±0.0044		Na^{22}	1.2736
Zn	30	1.5869±0.0045	1.5865±0.008	Na^{22}	1.2736

[a] D. E. Muller, H. C. Hoyt, D. J. Klein, and J. W. M. DuMond, Phys. Rev. **88**, 775 (1952).
[b] See reference 8.
[c] See reference 7.
[d] See reference 5.

The presence of a third low intensity γ ray ($3d_{3/2}\to2p_{3/2}$), and a calibration spectrum that is relatively far in energy from the mesonic x rays, adds what we feel are additional uncertainties in the $3d-2p$ measurements. These and the $3d-2p$ results along with their uncertainties are listed in Table II, with the breakdown of the uncertainties listed in Table V.

The relative weightings of the two $3d-2p$ x rays are in agreement with the $(2J+1)$ weighting predictions of the 0.50 for Pb and Tl, being (0.51 ± 0.02) and (0.53 ± 0.03), respectively. The value of Bi is somewhat high being (0.59 ± 0.02). This is probably due to the pronounced capture γ ray that was mentioned previously. This is discussed further in a later section.

C. $2p-1s$ Fe

TABLE IV. Uncertainty tabulations for $2p-1s$ transitions of Tl, Pb, Bi, and Fe.

Experimental quantity	Element	χ^2 analysis	Source energy	Relative position of calibration and x-ray spectra	Total
$2p_{3/2}-1s$ energy (MeV)	Tl	0.0073	0.006	0.006	0.011
	Pb	0.0064	0.006	0.006	0.011
	Bi	0.0034	0.006	0.006	0.009
$2p-1s$ energy (MeV)	Fe	0.00098	0.0018	0.00127	0.0024
Δ_{2p}	Tl	0.0043	···	···	0.0043
	Pb	0.0060	···	···	0.0060
	Bi	0.0042	···	···	0.0042

TABLE V. Uncertainty tabulations for $3d-2p$ transitions in Tl, Pb, and Bi.

Experimental quantity	Elements	χ^2 analysis	Source energy	Relative position of calibration and x-ray spectra	Slope of pulser calibration	Presence of third x-ray	Resolution difference	Total
$E(3d_{5/2}-2p_{3/2})-0.1\Delta_{3d}$ (MeV)	Tl	0.0034	0.001	0.0025	0.0015	0.002	0.002	0.0054
	Pb	0.0015	0.001	0.0025	0.0013	0.002	0.002	0.0044
	Bi	0.0018	0.001	0.0026	0.0012	0.002	0.0015	0.0043
$\Delta_{2p}-0.9\Delta_{3d}$	Tl	0.0030	···	···	0.0008	0.002	0.003	0.0048
	Pb	0.0030	···	···	0.0006	0.002	0.0025	0.0044
	Bi	0.0021	···	···	0.0005	0.002	0.002	0.0036

The expected fine structure splitting of Fe is much too small to be observed, so the fine structure splitting and relative weightings of the two x rays are omitted, enabling one to use a four parameter χ^2 analysis. The calibration γ ray is the (1.2736±0.0018)-MeV γ ray[7] from Na^{22}. The χ^2 analysis covered 16 channels with the minimum χ^2 being 11.8 compared to the expected value of 12±4.9. The results are listed in Table III, with the uncertainty breakdown in Table IV. The $2p-1s$ spectrum is shown in Fig. 14 along with the best fit synthesized curve.

D. $2p-1s$ Ti, Cu, and Zn

The calibration γ rays were not close enough in energy to the $2p-1s$ mesonic atom x rays to justify a χ^2 analysis for these elements. The calibration curves and mesonic atom x-ray spectra were symmetric enough so that a peak channel could be determined to $\pm\frac{1}{4}$ channel by averaging over several points on the high and low side of the spectrum. Thus, the energy uncertainties in these $2p-1s$ transitions arise from (a) the $\pm\frac{1}{4}$ channel uncertainty in the x-ray and calibration spectra, (b) the relative position of the x-ray and calibration spectra as determined from the monitor γ-ray spectrum, (c) the calibration source energy uncertainty. The calculated results with their uncertainties are listed in Table III with the uncertainty breakdown given in Table VI. The $2p-1s$ spectra are shown in Figs. 15, 16, 17 for Ti, Cu, and Zn, respectively.

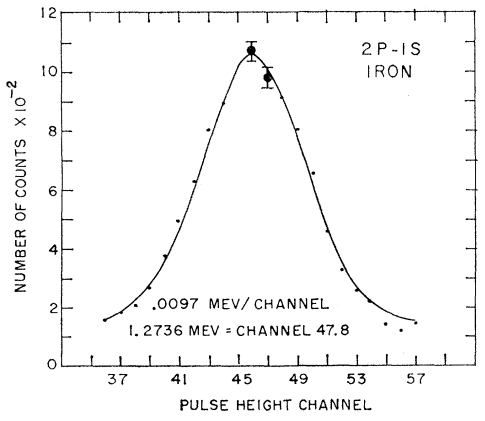

FIG. 14. Experimental results for the $2p-1s$ transitions in Fe. The smooth curve represents the best-fit synthesized curve for which $\chi^2=11.8$.

A comparison of the χ^2 values with the expected values suggests that there is a systematic tendency for the experimental χ^2 values to be less than that expected solely from statistical considerations. While this is preferable to the opposite sign of deviation, it needs some explanation. One effect that may be involved is the smoothing effect of the folding procedure in reducing the random fluctuations of adjacent points. We have made no attempt to estimate this effect precisely, but it does not seem unreasonable that it could give the observed lower χ^2 values. It should not otherwise influence the experimental results.

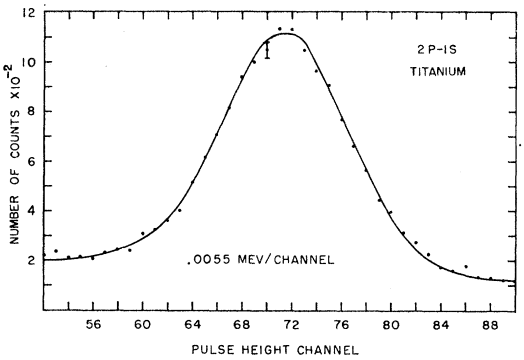

FIG. 15. Experimental results for the $2p-1s$ transistions in Ti.

IV. CONCLUSIONS

A. Relative Weightings

The $3d-2p$ results for Tl and Pb yield the expected $(2J+1)$ relative weightings for the $2p_{3/2}$ and $2p_{1/2}$ states. The value for Bi was 0.59±0.02, which is somewhat high. This can probably be accounted for by the presence of a very pronounced capture γ ray of ~2.6 MeV. Our interpretation of the origin of this γ ray is as follows:

$$\mathrm{Bi}^{209}+\mu^- \rightarrow \mathrm{Pb}^{209*}+\nu$$
$$\qquad\qquad\quad \downarrow$$
$$\qquad\qquad\quad \rightarrow n+\mathrm{Pb}^{208*}.$$

TABLE VI. Uncertainty tabulations for $2p-1s$ transitions in Ti, Cu, and Zn. Energies in MeV.

Element	Calibrating source	Calibrating source energy	Calibration source peak channel 1	Mesonic x-ray peak channel	Relative positions of calibration and x-ray spectra	Total
Ti	Cs^{137}	0.00014	0.0019	0.0014	0.0009	0.0025
Ti	Mn^{56}	0.015	0.0015	0.0014	0.0009	0.015
Cu	Na^{22}	0.0018	0.0029	0.0024	0.0015	0.0044
Cu	Na^{24}	0.0010	0.0027	0.0024	0.0015	0.0040
Zn	Na^{22}	0.0018	0.0030	0.0024	0.0016	0.0045

The first excited state in Pb^{208} is a 2.615-MeV 3^- level,[9] and this level radiating to the ground state is believed to provide the capture γ ray that is observed in Bi^{209}. This capture γ ray is measured to occur with approximately one-half the intensity as the mesonic x rays, of which 10% are not time discriminated against. The energies of the two $3d \rightarrow 2p$ mesonic x rays are 2.55 and 2.70 MeV. Thus, the capture γ-ray energy falls between the two mesonic x rays raising the knee on the high-energy side of the $3d-2p$ spectrum enough to effect an increase from 0.5 to 0.59 for the measured relative weighting.

The relative weightings of the $2p_{1/2}$ and $2p_{3/2}$ levels obtained from Pb is 0.49 ± 0.07 in agreement with the expected weightings. However, the relative weightings for Tl and Bi are 0.97 ± 0.09 and 0.75 ± 0.05 which are well above the expected values beyond any experimental uncertainty. Capture γ rays were suspected as the cause of this effect when it was first observed in the earlier series of measurements and was the reason why we took special care to examine the capture γ-ray spectrum in the series of measurements herein reported. The tests definitely ruled out this possibility. On the basis of strictly atomic transition phenomena it is very difficult to see how, if any deviation of W from the expected value were found, it could differ significantly for Tl, Pb, and Bi. There is the further important fact that

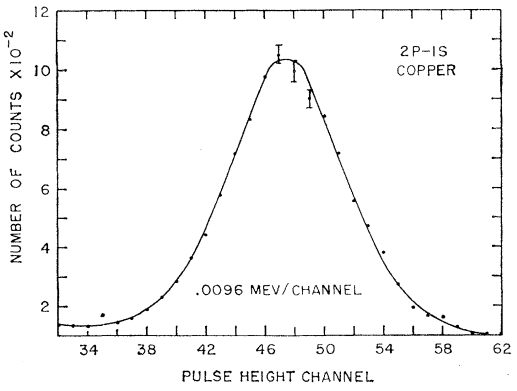

FIG. 16. Experimental results for the $2p-1s$ transitions in Cu.

essentially the expected weightings of transitions *to* the $2p_{3/2}$ and $2p_{1/2}$ states were obtained from the $3d \rightarrow 2p$ weightings. After much worrying over this point, we now tentatively favor the following explanation which we have not checked quantitatively, but which could qualitatively explain the experimental results. The 70% abundant Tl^{205} nucleus has an $s_{1/2}$ ground state and a $d_{3/2}$ first excited state of 0.205-MeV excitation.[10] This is very close to the splitting of the $2p$ states so one might expect a quadrupole type coupling between the μ meson and the nucleus to cause the nominal $2p_{3/2}$ muon state to become a linear combination of $2p_{3/2}$ muon with ground-state nucleus plus $2p_{1/2}$ muon with $d_{3/2}$ excited-state nucleus. The $2p_{1/2}$ muon with ground-state nucleus would remain relatively pure. The parity of the ground and excited states and rules on angular momentum coupling are consistent with this interpretation of the mixed character of the 3/2 state which would usually just the $2p_{3/2}$ muon state. If the 3/2 and 1/2 states are now populated in a 2 to 1 ratio as expected and as found from the $3d \rightarrow 2p$ results, the $2p \rightarrow 1s$ transition from the 1/2 state would behave normally, but the "$2p_{3/2}$" $\rightarrow 1s$ transition would result in leaving the nucleus in its 0.205-MeV excited state a significant fraction of the time with an x-ray energy release almost identical to that of the lower energy $2p_{1/2} \rightarrow 1s_{1/2}$ transition to give the latter a seemingly large weighting as observed.

In the case of Pb, which is mainly Pb^{208}, the first excited state is at 2.165 MeV and is a 3^- state. This state has the wrong parity, in addition to its very large energy difference from the ground state, to provide such an effect for Pb. It is thus gratifying that Pb shows essentially the predicted value for W. In the case of Bi^{209} the deviation of W is intermediate between the originally expected value and that for Tl. The ground state of Bi^{209} is $h_{9/2}$ and the first excited state, of 0.91-MeV excitation, is an $f_{7/2}$ state.[10] While 0.91 MeV is large compared to the fine structure splitting, the larger angular momentum of Bi probably tends to increase the quadrupole matrix strengths so it is conceivable that it may provide the correct explanation of the observations. A careful quantitative theoretical evaluation of these effects is much to be desired.

[9] L. V. Groshev, V. N. Lutsenko, A. M. Demidov, and V. I. Pelekhov, *Atlas of γ-Ray Spectra from the Radiative Capture of Thermal Neutrons* (Pergamon Press, New York, 1959), p. 182.

[10] D. Strominger, J. M. Hollander, and G. T. Seaborg, Revs. Modern Phys. **30**, 585 (1958).

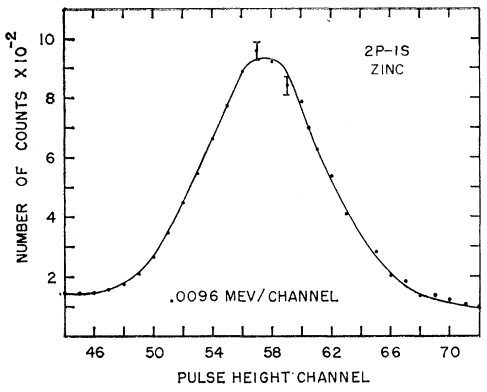

FIG. 17. Experimental results for the $2p-1s$ transitions in Zn.

B. Energy and Fine Structure

The theoretical calculations which we have used are those of Ford and Wills.[2] which represent elaborate numerical solutions of the Dirac equation. They used a nuclear charge distribution suggested by the high-energy electron scattering experiments,[11] and included vacuum polarization corrections, but not nuclear polarizability contributions. These theoretical $2p-1s$ energies for Tl, Pb, and Bi are claimed to have an 0.8% uncertainty due to uncertainties in the nuclear charge distribution. The $2p-1s$ transition energies for the lower Z elements and the $3d-2p$ energies near $Z=82$ should be less sensitive to the nuclear charge distribution. The uncertainty in nuclear polarizability effects may be more important in these cases and may vary appreciably from nucleus to nucleus depending on the detailed form of the low-lying nuclear states and their energies. Our results are in good agreement with these theoretical predictions. The comparison with theory and experiment is shown in Fig. 18 for the $2p-1s$ transitions. The $2p-1s$ results for Ti, Fe, Cu, and Zn are all higher than theory predicts, but with the exception of Fe, which is 1.3% too high, all agree within the theoretical and experimental uncertainties. This discrepancy may be accounted for by the Cooper-Henley[12] estimate of the nuclear polarization effect, which could if included, increase the theoretical energy by $\sim 1\%$. Their estimates might be too high in some cases and too low in others, however, depending on the detailed character of the low-lying nuclear excited states. This might explain why Zn is in agreement with predictions, while Fe is 1.3% too high. A more precise calculation of the effects of quadrupole couplings of the muon and the nucleus would be required to test this possibility.

The values of Δ_{2p} and $(\Delta_{2p}-0.9\Delta_{3d})$ are in excellent agreement with the theoretical values. The high Z $2p_{3/2}-1s$ energies are in essential agreement with theory. The Tl value is 1.3 standard deviations too low, and the Pb value is 0.7 standard deviation too high. The Bi value is 1.0 standard deviations higher than the Ford and Wills (F-W) predicted values. While this alone would indicate no disagreement, we have both experimental and theoretical reasons for believing that the F-W choice for the nulcear charge distribution should be modified. Table VII shows their choice of the nuclear size and shape parameters and the resulting energies for W, Tl, Pb, Bi, and U. The energies are in MeV and the lengths in fermis. The value of r_1 determines the transition radius between the "inside" and "outside" functional forms for the nuclear charge density, while increasing n corresponds to increasingly narrow nuclear edge regions. $R_{eq}=[(5/3)\langle r^2\rangle]^{1/2}$ and n are the most interesting parameter values for this discussion. The values for W and U are included for two reasons: (a) They represent Z values reasonably but not excessively close to those of Tl, Pb, and Bi, to indicate the gross variation of the transition energies and Δ_{2p} in this region, (b) W and U are both far from closed shells and have large intrinsic quadrupole distortions, which would cause one to believe that much larger effective edge smearing values should be used for them than for the near double closed shell nuclei Tl, Pb, and Bi. We call attention to the n values in this table. Those of Tl and Pb are almost the same, i.e., about 10.0. The value chosen for Bi, however, is quite close to that chosen for W and is much smaller even than that for U. Since Bi^{209} is

TABLE VII. Ford and Wills parameters and results for their theoretical energy level calculations for W, Tl, Pb, Bi, and U.

				Energies (MeV)		
Z	$r_1/A^{1/3}$	n	$R_{eq}/A^{1/3}$	$2p_{1/2}-1s$	$2p_{3/2}-1s$	Δ_{2p}
74	1.10	7.50	1.23	5.220	5.362	0.142
81	1.10	9.90	1.18	5.817	6.001	0.184
82	1.11	10.00	1.19	5.837	6.025	0.188
83	1.094	7.70	1.22	5.807	5.995	0.188
92	1.10	8.50	1.21	6.304	6.538	0.234

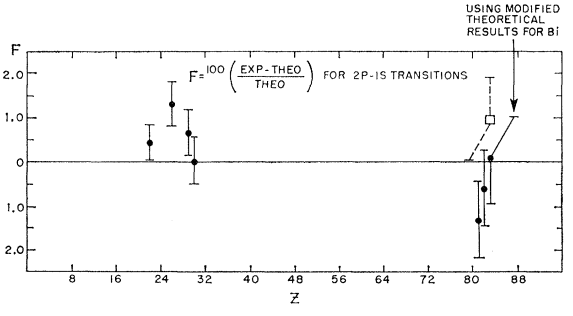

FIG. 18. Comparison of experimental results with the calculations of Ford and Wills. Both experimental and theoretical uncertainties contribute to the size of the indicated uncertainties with the greatest contribution to the uncertainty being associated with the theoretical calculations. The modified Bi value is related to a proposed modification of the theoretical values as suggested in the text.

[11] Cf., Papers from the International Congress on Nuclear Sizes and Density Distributions held at Stanford University, December 17–19, 1957, Revs. Modern Phys. **30**, 412 (1958).

[12] L. Cooper and E. Henley, Phys. Rev. **92**, 801 (1953).

Pb^{208} plus one proton, it seems more plausible *a priori* to form a smoother sequence of values for the energies in the Pb region. Thus, we suggest that "modified interpolated theoretical" values of $2p_{1/2}-1s=5.856$ MeV, $2p_{3/2}-1s=6.047$ MeV, and $\Delta 2p=0.191$ MeV are more reasonable for Bi than those obtained from the charge distribution assumed by Ford and Wills. The experimental results certainly favor a smooth sequence. The above suggested "modified theoretical" values are indicated by an asterisk in Table II.

C. Spin of the Muon

It becomes more and more difficult to argue convincingly for the possibility that the muon has other than spin 1/2. The main earlier arguments are given by Rainwater.[13] The supposed next favored possibility after spin 1/2 is spin 3/2. Here most theories[14] of spin 3/2 particles predict the g factor is $g=1/s=2/3$. This is clearly ruled out by recent precision measurements[15] of g and $(g-2)$ which show that g is exceedingly close to 2.0. Thus, if one uses an *ad hoc* spin 3/2 theory having $g=2$, there would be more lines of greater effective splitting than was observed experimentally. A reasonable approach to a spin 3/2 theory seems to be obtained by using the perturbation theory formula for the spin-orbit coupling:

$$E_{\text{F.S.}}=\langle f(r)\rangle_{n,l}\mathbf{L}\cdot\mathbf{S}.$$

Since $\langle f(r)\rangle_{n,l}$ depends only on n, l, and g but not on the muon spin, one obtains from the above formula

$$\Delta(2p_{1/2},2p_{3/2})=(3/5)\Delta(2p_{3/2},2p_{5/2})$$

for a spin 3/2 particle. The spin independence of $\langle f(r)\rangle_{n,l}$ enables one to set $\Delta(2p_{1/2},2p_{3/2})$ equal to the calculated value of 0.188 MeV for $Z=82$, and thus

$$\Delta(2p_{3/2},2p_{5/2})=0.313 \text{ MeV}.$$

A spin 3/2, $g=2$, muon would thus yield a $2p-1s$ spectrum that consists of $2p_{5/2}-1s$, $2p_{3/2}-1s$, and $2p_{1/2}-1s$ x rays separated by 0.313 and 0.188 MeV with relative weightings of 3/2/1, respectively. Hence, in addition to the synthesized spectrum shown in Fig. 9, one must add a third x ray of 0.313 MeV ($\sim$8 channels) higher energy and with 3/2 the intensity of the $2p_{3/2}-1s$ x ray. Such an x ray would have been easily detected if present.

Similar arguments can be applied to the $3d-2p$ transitions, (ignoring the $3d$ state splittings). A spin 3/2 muon would yield a $3d-2p$ spectrum that consists essentially of $3d-2p_{5/2}$, $3d-2p_{3/2}$, $3d-2p_{1/2}$ x rays with approximately 0.25- and 0.15-MeV sepration, and relative intensities of 3/2/1. Thus, in addition to the synthesized spectrum shown in Fig. 12 one must add a third x ray of 0.25 MeV ($\sim$12 channels) lower energy and 3/2 the intensity of the $3d-2p_{3/2}$ x ray. Again, if such an x ray were present, it would have been easily observed. The important point is that the third relatively high intensity x ray that would be emitted by a spin 3/2 muon is not observed. On the other hand, the experimental values of Δ_{2p} and $(\Delta_{2p}-0.9\Delta_{3p})$ are in excellent agreement with the Dirac spin 1/2 theory.

Note added in proof. Since the submission of this paper for publication, the following information of relevance to this paper has come to our attention:

(1) Professor K. W. Ford has informed us (private communication) that more recent electron scattering measurements for Bi support our position that essentially the same nuclear radius and edge diffuseness coefficients should apply for Tl, Pb, and Bi.

(2) P. Brix, R. Engfer, U. Hegel, D. Quitmann, G. Blackenstoss, K. Goebel, and D. Stadler, Physics Letters **1**, 56 (1962) give preliminary results for measurements of the $2p-1s$ μ-mesonic transitions energies for a number of elements. The fine structure splittings were not reported and uncertainties were not stated. The reported energies are in fair to excellent agreement with ours where a comparison is possible. In particular, they obtain a Bi—Pb energy difference for the $2p-1s$ transition energy in excellent agreement with our value.

ACKNOWLEDGMENTS

We are indebted to Professor K. Ford and J. Wills for calculating and making available to us prior to publication several of the μ-mesonic energy levels which were not available in reference 2.

We wish to express our gratitude to Professor H. Primakoff and Professor R. Serber for discussions concerning our postulate for explaining the different weightings of the $2p-1s$ x rays for Tl, Pb, and Bi.

Our thanks are also extended to Professor N. Kroll and Professor R. Serber for their enlightening discussions on spin 3/2 particles.

[13] J. Rainwater, Ann. Rev. Nuclear Sci. **7**, 1 (1957).
[14] P. A. Moldauer and L. M. Case, Phys. Rev. **102**, 279 (1956).
[15] R. L. Garwin, D. P. Hutchinson, S. Penman, and G. Shapiro, Phys. Rev. Letters **2**, 516 (1959); D. Hutchinson, J. Menes, G. Shapiro, A. Patlach, and S. Penman, *ibid.* **7**, 129 (1961); G. Charpak, F. J. M. Farley, R. L. Garwin, T. Muller, J. C. Sens, V. L. Telegdi, and A. Zichichi, *ibid.* **6**, 128 (1961).